Journal of
Manufacturing and Materials Processing

MDPI

Article

Design, Numerical and Experimental Testing of a Flexible Test Bench for High-Speed Impact Shear-Cutting with Linear Motors †

Pascal Krutz [1,*], André Leonhardt [1], Alexander Graf [1], Sven Winter [2], Elmar Galiev [2], Matthias Rehm [1], Verena Kräusel [2] and Martin Dix [1,2,*]

1 Institute for Machine Tools and Production Processes, Chemnitz University of Technology, Reichenhainer Str. 70, Building M, 09126 Chemnitz, Germany; andre.leonhardt@mb.tu-chemnitz.de (A.L.); alexander.graf@mb.tu-chemnitz.de (A.G.); matthias.rehm@mb.tu-chemnitz.de (M.R.)

2 Fraunhofer Institute for Machine Tools and Forming Technology IWU, Reichenhainer Str. 88, 09126 Chemnitz, Germany; sven.winter@iwu.fraunhofer.de (S.W.); elmar.galiev@iwu.fraunhofer.de (E.G.); verena.kraeusel@iwu.fraunhofer.de (V.K.)

* Correspondence: pascal.krutz@mb.tu-chemnitz.de (P.K.); martin.dix@mb.tu-chemnitz.de (M.D.)

† This paper is an extended version of our paper published in Pascal Krutz, André Leonhardt, Alexander Graf, Sven Winter, Matthias Rehm, Verena Kräusel, Martin Dix. Development and testing of a flexible test bench for high-speed impact shear-cutting with linear motors. In Proceedings of the 20th International Conference on Sheet Metal (SHEMET 2023), Erlangen-Nürnberg, Germany, 2–5 April 2023.

Citation: Krutz, P.; Leonhardt, A.; Graf, A.; Winter, S.; Galiev, E.; Rehm, M.; Kräusel, V.; Dix, M. Design, Numerical and Experimental Testing of a Flexible Test Bench for High-Speed Impact Shear-Cutting with Linear Motors. *J. Manuf. Mater. Process.* **2023**, *7*, 173. https://doi.org/10.3390/jmmp7050173

Academic Editors: Marion Merklein, Joost Duflou, Livan Fratini, Hinnerk Hagenah, Paulo A. F. Martins, Gerson Meschut and Fabrizio Micari

Received: 21 August 2023
Revised: 21 September 2023
Accepted: 23 September 2023
Published: 26 September 2023

Abstract: Given the use of high-strength steels to achieve lightweight construction goals, conventional shear-cutting processes are reaching their limits. Therefore, so-called high-speed impact cutting (HSIC) is used to achieve the required cut surface qualities. A new machine concept consisting of linear motors and an impact mass is presented to investigate HSIC. It allows all relevant parameters to be flexibly adjusted and measured. The design and construction of the test bench, as well as the mechanism for coupling the impact mass, are described. To validate the theoretically determined process speeds, the cutting process was recorded with high-speed cameras, and HSIC with a mild deep-drawing steel sheet was performed. It was discovered that very good cutting edges could be produced, which showed a significantly lower hardening depth than slowly cut reference samples. In addition, HSIC was numerically modelled in LS-DYNA, and the calculated cutting edges were compared with the real ones. With the help of adaptive meshing, a very good agreement for the cutting edges could be achieved. The results show the great potential of using a linear motor in HSIC.

Keywords: linear motor; blanking; high-speed impact shear-cutting; simulation

1. Introduction

The manufacturing of complex components and assemblies, such as vehicle bodies, requires additional punching operations after the actual forming process in order to be able to realize the final component geometry [1,2]. On the one hand, this includes the trimming of formed parts, and on the other hand, holes or forming contours are cut into the component to ensure further processing as well as the function of the component [3]. Therefore, a primary challenge is ensuring the required cut quality [4,5]. Given the growing importance of lightweight construction, higher, high-strength and ultra-high-strength steels are increasingly being used in vehicle construction [6], which means that the application limits of conventional shear-cutting operations are being reached [7]. One approach to optimising the shear-cutting of ultra-high-strength steels is to exploit high-speed effects in cutting processes [8]. In recent years, the potential of high velocities ($v \geq 10$ m/s) in shear-cutting has been investigated, analysed and evaluated within the framework of various research projects [9,10]. In so-called high-speed impact cutting (HSIC), early shear failure in the material is exploited by generating adiabatic shear bands [11–13]. Given this effect, even ultra-high-strength steels can be cut with particularly high-quality cut surfaces in a resource- and energy-efficient way [14,15]. The current hydraulic HSIC presses can provide very high-impact energies (up to 7000 J) and require a large installation space. However, recent studies show that significantly lower energies are required for cutting [16]. Winter et al. [17] were able to show, on the 3 mm thick and hardened steel 22MnB5, that 250 J impact energy and velocities significantly below 10 m/s are already sufficient to produce qualitatively very good cutting surfaces. Because significantly lower energies and velocities are sufficient, this allows for the use of other more flexible drive concepts with significantly smaller installation spaces. Electromagnetically accelerated drives are conceivable here, such as that of Linnemann et al. [18]. Therefore, an impact body is accelerated, which provides the impulse for the subsequent shear-cutting. However, the disadvantage is that the accelerated mass is usually below 5 kg; otherwise, the coils and the currents are very large, and consequently, the energy provided is also very low. Pneumatic [19] or explosively [20,21] operated drives are also conceivable. If larger masses are to be accelerated, however, they quickly reach their limits. Likewise, explosive drives are hardly transferable to larger industrial areas. Linear motors offer an interesting approach here because, in comparison with conventional drives, they can reach higher dynamics because of a lack of mechanical coupling elements [22]. As a result, highly dynamic motion profiles are achieved through significant accelerations, typically in the range of 100 m/s^2 [23]. These are mainly used in the areas of handling systems, machine tools and special machine building, as well as packaging and assembly systems [24]. Linear motors have a high degree of flexibility, are very compact and can easily accelerate masses significantly above 50 kg to the velocity range relevant for the HSIC ($v > 2$ m/s). Nevertheless, linear drives are not currently used for HSIC, as they are limited in their maximum force because of the physical principle of action and the associated lack of gearing on the one hand, and decoupling acceleration and impact is necessary on the other. This study will be the first to use the advantages of a linear actuator for HSIC. The paper is structured as follows: Section 2 outlines the conceptual design of the HSIC process, followed by explanations of its constructive realization and a summary of the test bench's benefits. At the end of Section 2, the experimental investigations to be performed are mentioned, with their execution and subsequent discussion presented in Section 3. Numerical validation of the cutting results through FEM analysis is performed in addition to experimental validation. The paper concludes with a summary of the main results.

2. Materials and Methods

2.1. Conception of the High-Speed Impact Cutting Process

The principle of a drop tower was adopted for the implementation of HSIC and is shown in simplified form in Figure 1, in which the process is divided into four phases. First, in phase one, a large impact mass (IM) is actively accelerated by a linear motor unit. During the transition to phase two, the IM is uncoupled from the motors and then continues to move downwards under the influence of acceleration due to gravity. Phase 3 describes the transfer of kinetic energy due to an elastic impact between the IM and a smaller, float-mounted mass—the shear-cutting tool. The mass ratio and the physical relationship of the elastic impact result in the higher speed of the tool with a mounted cutting punch, which should be in the adiabatic range. The final and fourth phase is meant to decelerate the moving components to a standstill. For the conceptual design of the test bench, the kinetic energies and the required cutting energies were calculated on the basis of the following equations. Equation (1) describes the kinetic energy of a mass, and Equation (2) represents the law of conservation of momentum, which can be used for calculations of the elastic impact of two masses [25].

$$E_{kin} = \frac{1}{2} m \cdot v^2 \tag{1}$$

$$\vec{p} = \sum_{i=1}^{n} m_i \cdot v_i = const. \quad (2)$$

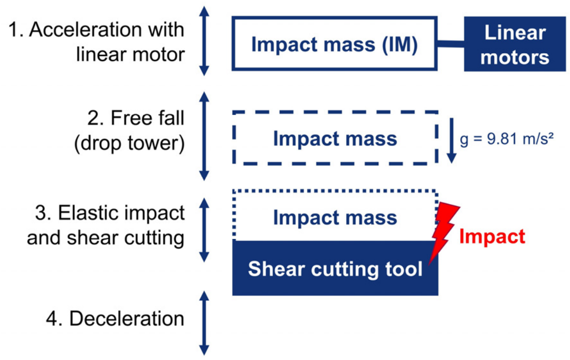

Figure 1. Simplified schematic representation of the HSIC concept.

Figure 2 describes the distribution of the different energies and their specific calculation. Initially, the kinetic energy of the IM is available based on the velocity, v_{IM0}, of the IM before the impact. After the impact, the kinetic energy of the IM splits into the remaining kinetic energy of the IM and the kinetic energy of the upper part of the cutting tool. The latter is available for the blanking process and is divided into the required cutting energy and the available energy for cutting speed. The quantity of this available energy finally determines the speed at which the cutting punch moves through the sheet metal strip in theory.

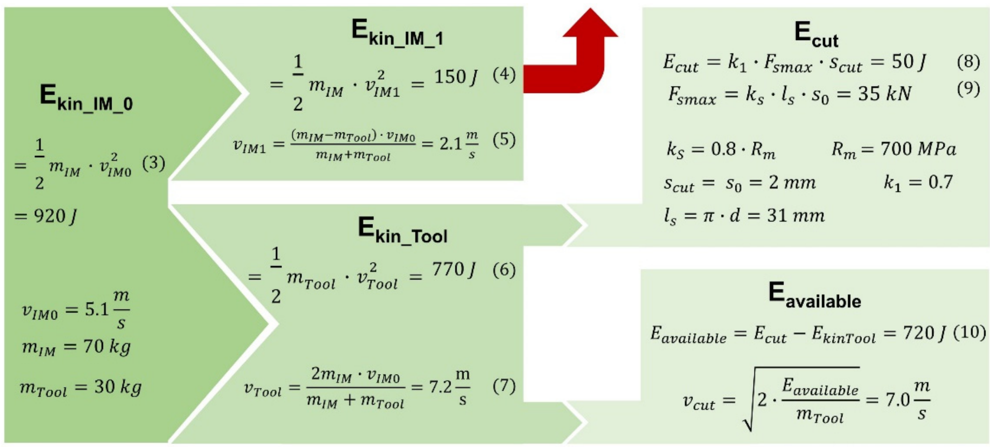

Figure 2. Allocation of the present process energies for conceptual design and their calculation, assuming the uncoupling speed of the linear motors to be 2 m/s.

The required masses of the IM and the cutting tool, as well as the required processing speeds, are inversely calculable via the theoretically occurring cutting speed. This should be in the adiabatic range for the generation of reproducible high-speed cutting effects on the workpiece. The calculation starts with the impact speed of the IM. This is composed of the nominal speed of the linear motors (set to 2.0 m/s) and a residual drop height (assumed to be 0.5 m). For the latter, a frictionless acceleration of 9.81 m/s^2 is assumed for simplification. With these assumptions, the impact velocity, v_{IM0}, amounts to 5.1 m/s. To calculate the velocities of the IM, v_{IM1}, and the cutting tool, v_{Tool}, after the impact, the equations of the elastic impact of the two masses are used. They are included in an adapted form in Figure 2. Since the IM has a significantly higher mass than the upper part of the cutting tool, the latter will move at a higher speed than the IM after the impact. In addition to the calculation of the kinetic energies, Figure 2 also shows the calculation of the cutting energy required for blanking a sheet metal strip (sheet thickness, s_0) with the length of the cutting line, l_s. The parameter k_1 is a scaling factor in a range of 0.4 to 0.7, and k_s describes the shear resistance that can be approximated with 0.8 tensile strength. After calculating the cutting energy and subtracting it from the kinetic energy of the cutting tool after the impact, the remaining amount is used to calculate the theoretical cutting punch speed. In this calculation example, the final cutting speed is around 7 m/s. In Table 1, the cutting speeds were calculated for other sheet materials with different tensile strengths, in each case for the three linear motor speeds, v_{mot}, 1, 1.5, and 2 m/s. It is evident that the enhancement of the sheet material's tensile strength has minimal impact on the theoretically achievable cutting speed. Conversely, elevating the motor speeds results in a considerable increase in the resulting cutting speeds.

Table 1. Calculated cutting speeds for different sheet materials and linear motor speeds.

Sheet Material (Tensile Strength)	v_{mot} = 1 m/s	v_{mot} = 1.5 m/s	v_{mot} = 2 m/s
Cu-OF R240 (240 MPa)	5.90 m/s	6.52 m/s	7.11 m/s
1.4404 (700 MPa)	5.71 m/s	6.35 m/s	6.95 m/s
HC450XD (780 MPa)	5.68 m/s	6.32 m/s	6.92 m/s

2.2. Constructive Realization of the Novel Test Bench

For practical implementation, a linear motor test bench was considered, which consists of two separately controllable, couplable linear motors. They can perform highly dynamic motions up to an acceleration of 100 m/s^2 because of their design and are thus predestined for the acceleration of the IM. For the integration of the shear-cutting tool into the linear motor test bench, depicted in Figure 3, a pillar-guided plate frame was chosen, into which the cutting tool was integrated. The plate frame includes top and base plates, which clamp four cylindrical guide pillars with a length of two meters. Two further plates are located between the top and base plates and are movable along the guide pillars with slide-bearing sockets. The more massive of these displaceable plates acts as the IM and has to be accelerated by the linear motors, whereas the second movable plate functions as a carrier for the cutting tool, subsequently referred to as the assembly plate. The two vertically movable linear motors move synchronously in gantry mode and are connected via an adapter plate. The technical data of the drives from SKF® are specified with a maximum force of 3.1 kN each and a maximum feed rate of 7 m/s at a nominal force and 2.3 m/s at maximum force.

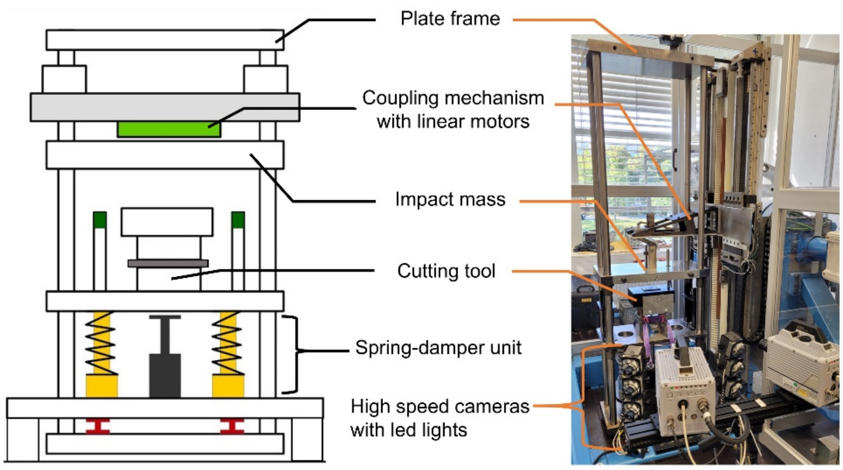

Figure 3. HSIC test bench—comparison of concept sketch and constructive realization.

The cutting tool is provided with an additional mass on the upper side to absorb an increased amount of kinetic energy from the IM during the elastic impact. After the impact of the cutting tool and the IM, the cutting punch immediately performs the shear-cut, and the cutting tool subsequently closes by itself. Next, the IM continues to move downwards at a reduced speed and is cushioned by two buffers. The buffers are also mounted on the assembly plate like the tool. This plate is floated with a spring-damper system in order to forward the dynamically occurring forces during the acceleration and deceleration of the components to the base frame.

For the pick-up of the IM, a linking mechanism was implemented that enables the detachment of the IM, which is necessary to protect the motors, as they must not collide with a stationary tool while the IM is linked. For this purpose, an arm was constructed on the adapter plate that enables the centric lifting and acceleration of the IM. The purpose of this is to prevent the potential wedging of bearing bushes and the guide pillars of the plate frame. The coupling mechanism was developed as a completely mechanical solution and is shown schematically in Figure 4. In (a), the lifting process is shown. The IM is lifted to the upper-end position by a bolt and a rotatably mounted hook (the red part in Figure 4a–c). In (b), the acceleration of the IM towards the tool is carried out. Given the high dynamic of the linear motors, the mounting of IM is first pushed against the base plate of the arm, which leads to the rotation of the hook. At the same time, the hook is locked by a fixator (the yellow part in Figure 4a–c) preloaded with a pressure spring. When the linear motors are subsequently decelerated, the IM continues to move unhindered until it collides with the tool. To recouple the impact mass, the locked hook moves downwards with the extension arm in (c). As soon as the hook reaches a defined distance from the IM, a release rod (the blue part in Figure 4c) pushes against the fixator, causing the hook to rotate downwards, and the IM is coupled. Afterwards, lifting the IM again can be carried out.

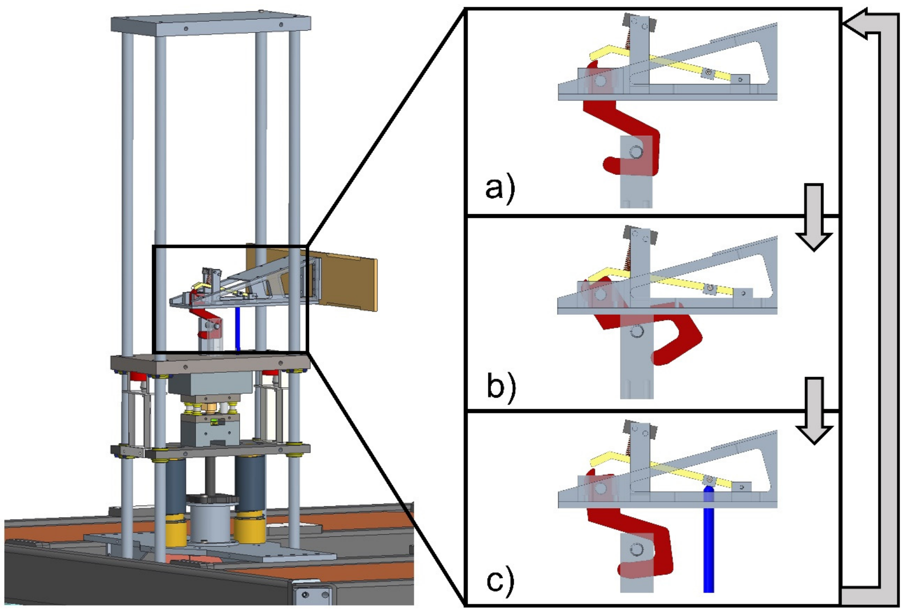

Figure 4. CAD model of the HSIC test bench with detailed representation of the linking mechanism ((**a**) lifting up, (**b**) acceleration/decoupling, (**c**) recoupling).

In accordance with Figures 3 and 4, the most important requirements for the test stand; their constructive realisation; and the resulting specific advantages are summarised in Table 2. The main advantage of the test bench is high flexibility in the examination of HSIC, as the applied impact energies can be continuously adjusted, and furthermore, good accessibility for the sensory recording of the shear-cutting process is guaranteed.

Table 2. Description of technological requirements; the corresponding constructive realisations; and the derivation of specific advantages.

Technological Requirement	Constructive/Technological Implementation
Highly dynamic acceleration of the cutting punch	Principle of elastic impact; acceleration of an impact mass with linear motors
Central localised impact on cutting tool	Selection of a frame with column-guided plates; one plate operates as the impact mass
Variation in the cutting energy	Flexible adjustment of the motor dynamics by setting control parameters; optional variation in impact mass and additional tool masses
Controlled absorption of dynamic forces	Use of a spring-damper system, which absorbs impact energy and transfers it to the frame over a large area
Linear motors must not collide with stationary masses	Construction of a coupling mechanism that enables the automated pick-up and uncoupling of the impact mass
Technological advantages compared with other test benches	

- Precise adjustment of impact energy by adjusting engine dynamics (speed, acceleration, jerk, setting of launch position) and variations in impact and cutting-tool masses;
- High accessibility for sensory acquisition of the HSIC process;
- Full mechanical implementation of the coupling mechanism without additional actuators;
- Recording of the cutting punch speed with high-speed cameras to ensure no obscuring of the field of vision by enclosures, etc.;
- Integrated motor-measuring system enables feedback on the applied impact energy;
- Easy access to the cutting tool simplifies workpiece handling.

In the following, the implemented automation and the technological sequences, shown in Figure 5, are described in more detail. At the beginning, the linear motors are in the start position. Here, the IM is located on the cutting tool in the uncoupled state. First, the linear motors move down to the IM and pick it up via the fully mechanical coupling mechanism. Afterwards, the IM is lifted by a few centimetres, while the upper part of the cutting tool, including the blank holder, is also lifted. This motion opens the cutting tool, and the sheet metal strip can be inserted. Subsequently, the cutting tool is closed, and the IM is lifted to the upper-end position of the linear motors. With release by the user, the IM accelerates up to the parametrised uncoupling speed. After uncoupling the IM, it is further accelerated by gravity until the elastic impact with the tool and the execution of the cutting process. After performing the shear-cutting operation and decelerating the moving masses with the spring-damper unit, one cycle is completed.

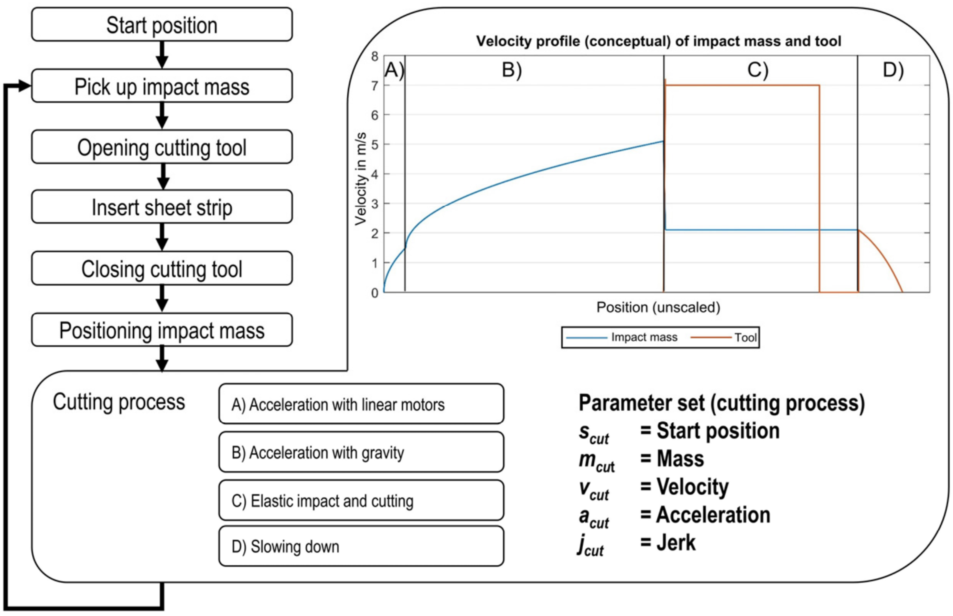

Figure 5. Technological flowchart for the implementation of HSIC trials.

In Figure 5, at the beginning of Section C, a pulse-like change in the speed of the IM and the cutting tool occurs. The speed of the cutting tool adjusts to the cutting speed, which results after the deduction of the required cutting energy. During the cutting process, the cutting punch moves faster through the metal strip than the IM falls at its residual speed. As a result, the cutting tool speed is temporarily at 0 m/s after the cutting process has been completed. As soon as the IM hits the buffers, both the IM and the cutting tool move downwards at the same speed and are decelerated by the spring-damper unit to a standstill.

2.3. Experimental and Numerical Studies

The first part of the investigation served to validate the test bench. For this purpose, motor speeds in a range of 1 to 2 m/s were tested. It was found that the correct uncoupling and recoupling of the IM occurred. Furthermore, we tested whether the accessibility of the loading tool was sufficient. In order to validate the theoretically occurring process speeds, the speeds of the IM and the upper part of the tool were recorded with high-speed cameras in three recording windows. The highly dynamic process of accelerating and decoupling the IM was also recorded for three motor speeds.

To validate the flexible test bench, circular blanks with a 10 mm diameter were cut from mild deep-drawing steel (1.0338, DC04). The fixed parameters for the test series included a sheet thickness (s = 2 mm), a related clearance (u_s = 2.5%s) and the specified material. The only variation during the validation process was the cutting speed, which depended on the decoupling velocity from the IM (1.0, 1.5 and 2.0 m/s). Additionally, conventional shear-cutting tests were conducted at a cutting speed of 0.025 m/s. Following the completion of the tests, the cut surfaces were evaluated in accordance with VDI 2906 sheet 2 [26]. Furthermore, the assessment of cut surface quality was enhanced by determining the hardening depth and conducting microstructural investigations.

Finally, an FE simulation of the HSIC was performed with the explicit mechanical solver R13.1 of the commercial software LS-DYNA (DYNAmore GmbH, Germany). The goal was to verify if the cut surface quality could be predicted with sufficient accuracy at high speeds. The plastic deformation behaviour of the material was described using the classic *MAT 024 PIECEWISE LINEAR PLASTICITY model, with the various strain-rate-dependent yield curves of DC06 steel (1.0873), which is nearly identical to the steel used in the experiment, DC04 (1.0338). Details of this model, including the yield curves used, are provided in [27]. Strain-rate-dependant damage and failure were modelled using the GISSMO damage and failure model developed by Neukamm et al. [28]. This model combines the damage description used to compute crash simulations and an incremental formulation to describe material instability and localisation. This fracture model can be used as a complement to the plastic material model and is specified using the *MAT_ADD_EROSION file. More detailed parameters for this fracture model are presented in [29]. Since the experiment used a circularly symmetric die, an axially symmetric 2D model was used to reduce computation time, as shown in Figure 6. The modelling was performed using an element formulation, numbered 15, with an element size of 0.05 mm. In addition, the new adaptive r-type mesh generation available in LS DYNA for 2D models was used to obtain a valid shear surface. All elements except the sheet (2 mm thick) itself were set as rigid bodies. The blank holder force was set to 10 kN; the friction coefficient was set to 0.15; and the clearance was 50 µm (related clearance = 2.5%s). The punch speed obtained from the experiment (3.0 m/s) was specified as input information for the simulation using the *BOUNDARY_PRESCRIBED_MOTION file.

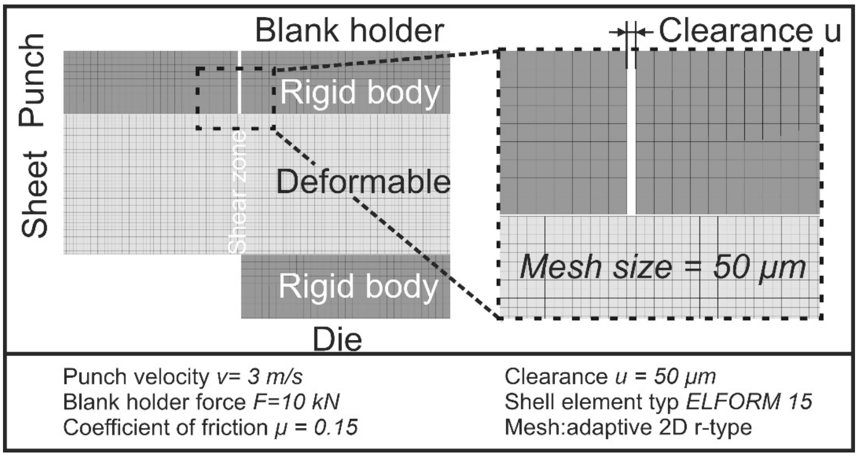

Figure 6. Two-dimensional axisymmetric model of the punching setup with relevant parameters and local mesh sizes for the FE simulation.

3. Results and Discussion

3.1. Validation of the Test Bench

After the successful commissioning of the test bench, the functionality of the conceptualized kinematics had to be proven. This includes, in particular, the effective coupling and decoupling of the IM for different process speeds. Two high-speed cameras were used in combination with two high-power LED spotlights to determine the process speeds of the IM and the tool. Figure 7 shows the determined velocity curves of the IM for an uncoupling velocity of 2.0 m/s. The sections (A) to (D) of the process depicted in Figure 5 were also included in Figure 7, although (C) and (D) cannot be separated exactly from each other in the measured curves. Since the entire motion range cannot be captured with one measuring range of the camera, three relevant measuring ranges, each covering 130 mm in the vertical direction, were selected. The arrangement of the first two upper windows was selected in such a way that, starting with the acceleration of the IM from a standstill, its speed was recorded approximately continuously over 260 mm. The set speed of the motors was already reached in the first window, with the result that only acceleration due to gravity is shown in the second window. After passing out of the second window, the IM continued to move downwards and is recorded with the third window subsequently at the impact height. The intermediary velocity curve is linearly interpolated according to the assumption of uniform acceleration and constant friction and is shown with an interruption (dotted lines in Figure 7) for the improved visibility of the subsequent camera window in Figure 7. Window 3 shows the first maximum speed of the tool at approximately 3.0 m/s, indicating that the adiabatic cutting range is reached. At 3.5 m/s, the impact velocity of the IM is around 1.6 m/s below the theoretically calculated impact velocity, v_{IM0}, in Figure 2. The main reasons for this are the frictional forces acting during the acceleration of the IM. These were not considered in the conception. If the calculation of the cutting speed is repeated with the measured impact speed, the result is 4.5 m/s for the v_{cut}. This implies that the v_{cut} is still 1.5 m/s below the calculated speed. This deviation can be partly explained by a lack of lossless energy transmission during the elastic impact. In particular, the floating mounting of the tool contributes to the absorption of parts of the kinetic energy by the IM from the spring-damper system. With good approximation, the recalculated velocity, v_{IM1}, of 1.4 m/s agrees with the practically measured velocity of the IM after the impact. After the impact of the IM with the tool, both velocity curves show an oscillating course. The oscillation behaviour can be explained by a superposition of several effects. First, the entire test bench is excited to oscillate as a coupled spring-mass damper system by the highly dynamic motion of the linear motors and the IM. During the motion of the IM and the tool plate, stick-slip effects also occur between the slide-bearing sockets and the guide pillars. Finally, the multiple impacts also lead to the occurrence of vibrations. The observed effects and measured process speeds indicate that the simplified assumptions made for the conceptual design of the cutting process are only valid within a limited range.

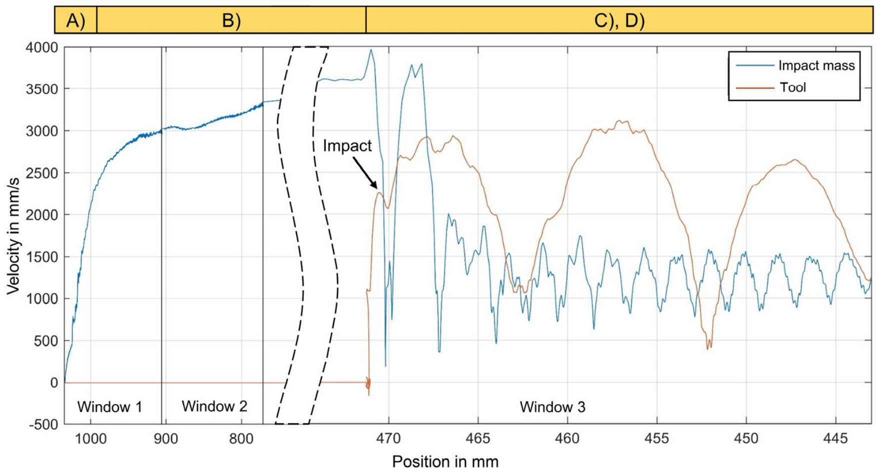

Figure 7. Measured velocity profile of the IM and tool, captured with three different recording windows, consisting of acceleration with linear motors (**A**), acceleration via free fall (**B**) and impact with the tool for a set uncoupling speed of 2 m/s (**C**,**D**).

During the cutting experiments, high-speed cameras were used to capture the decoupling process. Figure 8 shows one motion shot each at the tested decoupling speeds of 1.0, 1.5 and 2.0 m/s. For 1.0 m/s, it was determined that the mounting of the IM does not push against the base plate of the arm (see yellow box in Figure 8). Nevertheless, the resulting rotation angle of the hook is large enough that the fixation of the hook is achieved. However, at uncoupling speeds below 0.8 m/s, the resulting dynamics were too low, so the IM was partially not uncoupled. Adjusting the acceleration and jerk parameters would probably move this limit further down, but the resulting energy input could be too low to reach the adiabatic range; therefore, only decoupling speeds greater than or equal to 1 m/s were further investigated. With decoupling speeds of 1.5 m/s and 2.0 m/s, the mounting of the IM comes into contact with the base plate of the arm and leads to the oscillation of the entire arm, increasing at higher speeds. This effect is also visible in Figure 8, where the fixator rotates further away from the hook contour with increasing speed. For a further expansion of the uncoupling speed, a constructive stiffening of the arm geometry, as well as an increase in the compression spring stiffness, should be taken into consideration. However, for the investigated parameter range of 1.0 to 2.0 m/s for the decoupling speed, the functionality of the described construction for picking up and decoupling the IM can be fully demonstrated.

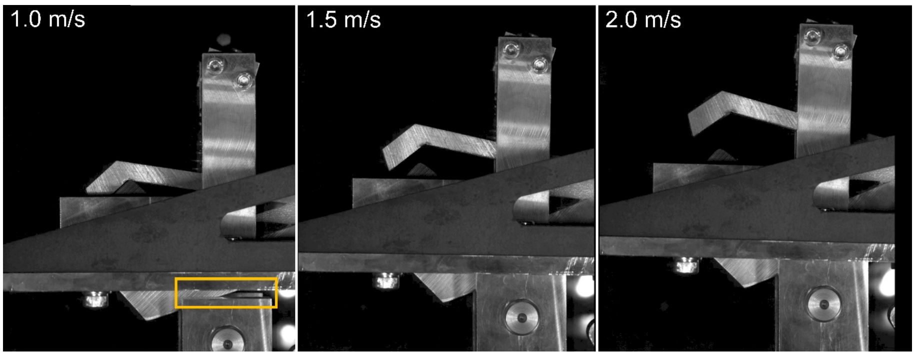

Figure 8. High-speed recording of the uncoupling process of the IM, shown for three different uncoupling speeds, highlighting the remaining distance between the base plate of the arm and the mounting of the IM at 1.0 m/s in the yellow box.

3.2. Experimental and Numerical Validation of the HSIC Process

A crucial step in evaluating the results of shear-cutting is determining the shear-cutting speed. Figure 9 illustrates the linear relationship between the punch speed and the decoupling velocity of the IM. The measurement results yield the following punch velocities: 2.5, 2.8 and 3.0 m/s. This also enables the assessment of the cut surface quality as a function of shear-cutting speed (Figure 10), though only three cutting speeds (0.025, 2.5 and 3 m/s) are represented. It is evident that rollover diminishes with increasing cutting speed. Conversely, the proportion of the clean-cut zone decreases, consequently increasing the fraction of the fracture zone with higher cutting speed. Another positive aspect is the increase in the fracture surface angle when using HSIC. All results share a significant transition from v = 0.025 m/s to v = 2.5 m/s, but a saturation point or even a reversal of results occurs with a further increase in cutting speed.

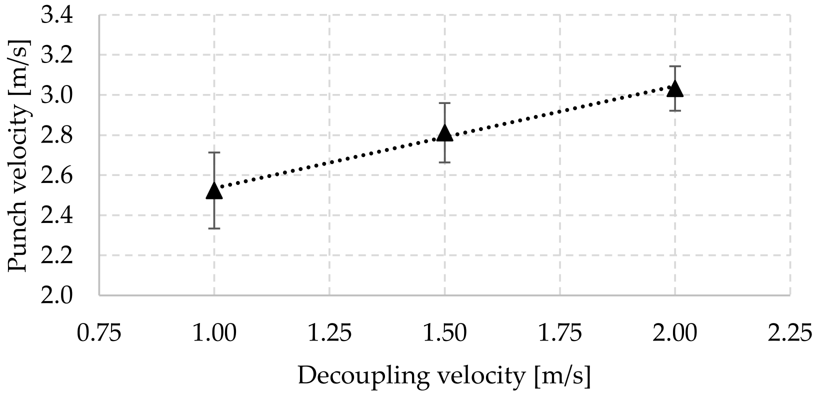

Figure 9. Representation of the linear relationship between the measured decoupling velocity and the measured punch velocity (mean values shown as triangles and standard deviations as bars).

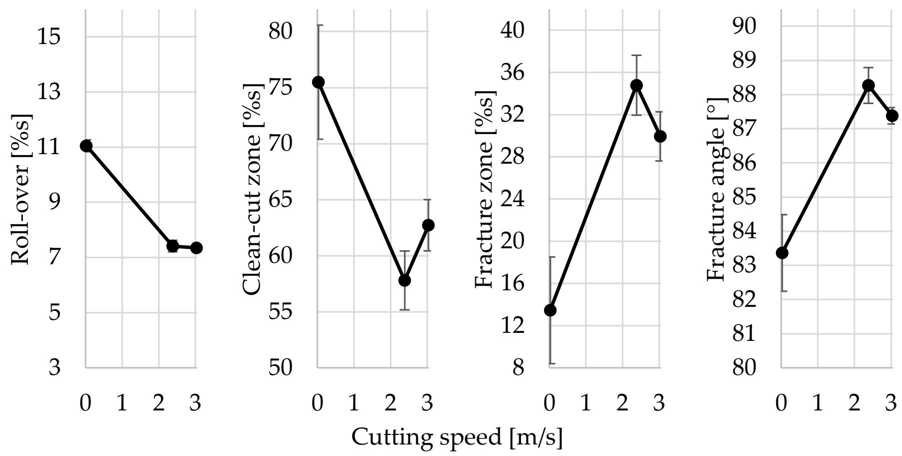

Figure 10. Influence of the cutting speed on the cutting surface characteristics.

When characterizing the microstructure through hardness mapping, additional effects of punch velocity become evident. At a punch speed of 0.025 m/s, there is observable increased hardening towards the cutting edge (Figure 11a). The hardening depth extends up to 0.5 mm from the cutting edge. When the punch speed increases to 3.0 m/s, the hardening depth decreases to 0.3 mm (Figure 11b). Notably, there is a smaller increase in hardness in the region from the rollover to the beginning of the fracture zone when compared with a punch speed of 0.025 m/s. Upon examining the microstructure (Figure 11c), it becomes evident that significant deformation has occurred in this region, indicating the presence of an adiabatic shear band in this area.

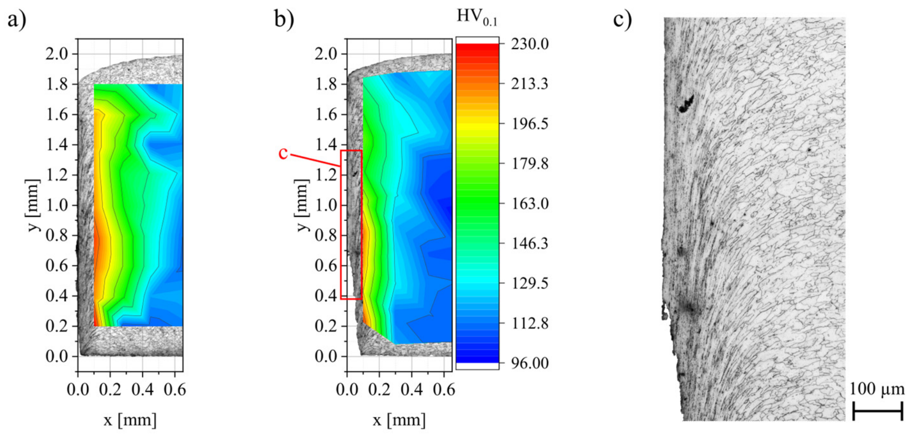

Figure 11. Measured hardening profiles for variations in the punch speed: (**a**) 0.025 m/s, (**b**) 3 m/s and (**c**) the enlargement of the microstructure in the area of large deformation at 3 m/s.

The FE simulation results are shown in Figure 12 as three phases of cutting. Figure 12a,b show the formation of the clean-cut directly in the HSIC with the highest local strains in the area of the tip of the punch. The width of the rollover is significantly smaller compared with the real results (see Figure 11b). Figure 12c shows the resulting cut surface after HSIC. The clean-cut in the simulation is 1.20 mm, and the fracture zone is 0.67 mm. The fracture surface could not be perfectly modelled from the geometric shape (especially the angle) despite the extensive GISSMO damage model and adaptive meshing. The inclination of the fracture zone is significantly larger at the real cut surface (see Figure 11b). Nevertheless, the absolute values of the clean-cut and the fracture zone are in very good agreement with the real values from the experiment, where the clean-cut was 1.18 mm, and the fracture zone was 0.68 mm (see Figure 11b). Adding the values of the clean-cut and the fracture zone results in a simulation cut area of 1.87 mm and a real cut area of 1.86 mm. These values are just below the initial sheet thickness of 2.0 mm. This is due to the fact that the height of each rollover is not taken into account. In addition, the width of the rollover is significantly smaller in the simulation than in the real cut area. As a result, the simulation model used is very good at predicting the quality of the resulting cut surfaces.

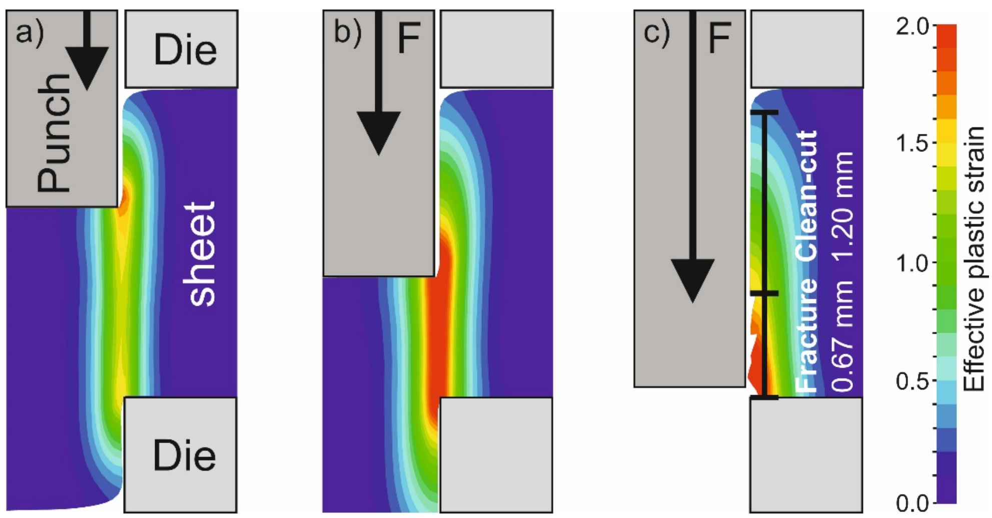

Figure 12. Results of FE simulation with evaluation of clean-cut and fracture zone: (**a**,**b**) show the formation of the clean-cut zone with the highest local strains during HSIC; (**c**) shows the clean-cut and fracture zone after HSIC with the resulting measured values.

3.3. Discussion

HSIC tests were carried out with the presented test bench. Linear motors in combination with a drop tower were used to generate cutting energy. The implemented coupling mechanism enabled the IM to be coupled and uncoupled for different process speeds. The deceleration of the moving masses to a standstill was reliably achieved by the described spring-damper mechanism. The motor control enables the precise presetting of the nominal speed of the motors. Consequently, the energy input for performing the cutting process and the resulting cutting speeds can be adjusted with fine granularity. The construction, which is easily accessible for sensor technology, enabled the precise measurement of occurring tool velocities and, therefore, the comprehensive investigation of HSIC.

Three different decoupling velocities (1.0, 1.5 and 2.0 m/s) were investigated for a mild, deep-drawing steel. The determined IM and tool velocities were lower than the conceptually calculated velocities, which was mainly due to the effect of frictional forces and energy losses during impact. In the verification of the cutting results, a high punch speed (up to 3.0 m/s) was proven. This is reflected in the influence on the quality of the cut surface and the microstructure. Finally, HSIC was numerically modelled, and the cut surfaces of the steel used were compared between real and numerical results. A very good agreement was found.

4. Conclusions

In the presented work, a novel approach to the HSIC process was implemented. The highly dynamic acceleration capacity of linear motors was used to accelerate an impact mass. According to the drop tower principle, the accelerated mass impacts a shear-cutting tool. The tool is accelerated by the elastic impact, and the cutting process is executed. After an initial conceptual calculation of the resulting process speeds, the constructive realisation was presented, and the successive movement sections were specified. Subsequently, the test bench was validated by examining the coupling and uncoupling processes for different process speeds.

Verification of the cutting results showed the remarkable effectiveness of high punch speeds, particularly when applied to mild steel, reaching speeds of up to 3.0 m/s. These high punch speeds had a profound effect on both the quality of the cut surface and the microstructure. In addition, the successful numerical modelling of the HSIC process enabled a comprehensive comparison between actual cut surfaces and their numerical counterparts. This analysis revealed an exceptionally close match between the two, further validating the accuracy and applicability of the proposed approach.

In the continuation of the presented investigations, the speed of the falling mass will be further increased, with a main focus on reducing friction on guide columns. To further expand the process, we also plan to cut other materials, such as high-strength steels.

Author Contributions: Conceptualization, M.R., P.K., A.G. and A.L.; investigation and validation, P.K., S.W., M.R., A.G. and A.L.; formal analysis, S.W., E.G., P.K., A.G. and A.L.; writing—original draft preparation, P.K., S.W., M.R., A.G. and A.L.; writing—review and editing, M.D. and V.K.; project administration, M.D. and V.K. All authors have read and agreed to the published version of the manuscript.

Funding: This research received no external funding.

Data Availability Statement: The data are not publicly available.

Conflicts of Interest: The authors declare no conflict of interest.

References

1. Kindsmüller, A.; Schrepfer, A.; Stahl, J.; Pätzold, I.; Nürnberger, A.; Golle, R.; Volk, W. Influence of Cutting Parameters on Mechanisms Causing Slug Pulling. *Prod. Eng.* **2021**, *15*, 833–842. [CrossRef]
2. Zeidi, A.; Ben Saada, F.; Elleuch, K.; Atapek, H. AISI D2 Punch Head Damage: Fatigue and Wear Mechanism. *Eng. Fail. Anal.* **2021**, *129*, 105676. [CrossRef]
3. Karbasian, H.; Tekkaya, A.E. A Review on Hot Stamping. *J. Mater. Process. Technol.* **2010**, *210*, 2103–2118. [CrossRef]

4. Lu, J.; Khawarizmi, R.; Monclús, M.; Molina-Aldareguia, J.; Kwon, P.; Bieler, T.R. Effect of Cutting Speed on Shear Band Formation and Chip Morphology of Ti–6Al–4V Alloy Using Nanoindentation and EBSD Mapping. *Mater. Sci. Eng. A* **2023**, *862*, 144372. [CrossRef]
5. Bohdal, Ł.; Patyk, R.; Tandecka, K.; Gontarz, S.; Jackiewicz, D. Influence of Shear-Slitting Parameters on Workpiece Formation, Cut Edge Quality and Selected Magnetic Properties for Grain-Oriented Silicon Steel. *J. Manuf. Process.* **2020**, *56*, 1007–1026. [CrossRef]
6. Merklein, M.; Wieland, M.; Lechner, M.; Bruschi, S.; Ghiotti, A. Hot Stamping of Boron Steel Sheets with Tailored Properties: A Review. *J. Mater. Process. Technol.* **2016**, *228*, 11–24. [CrossRef]
7. Lipiäinen, K.; Afkhami, S.; Ahola, A.; Björk, T. Evaluation of Geometrical Notch and Quality Effects in the Fatigue Strength Assessment of Ultra-High-Strength Steel Cut Edges. *Structures* **2022**, *37*, 881–892. [CrossRef]
8. Gu, L.; Kang, G.; Chen, H.; Wang, M. On Adiabatic Shear Fracture in High-Speed Machining of Martensitic Precipitation-Hardening Stainless Steel. *J. Mater. Process. Technol.* **2016**, *234*, 208–216. [CrossRef]
9. Hu, D.; Chen, M.; Wang, L.; Wang, H. Microstructural Characterization of Blanked Surface of C5191 Phosphor Bronze Sheet under Ultra-High-Speed Blanking. *Trans. Nonferrous Met. Soc. China* **2021**, *31*, 692–702. [CrossRef]
10. Gaudillière, C.; Ranc, N.; Larue, A.; Lorong, P. Investigations in High Speed Blanking: Cutting Forces and Microscopic Observations. *EPJ Web Conf.* **2010**, *6*, 19003. [CrossRef]
11. Rittel, D.; Wang, Z.G.; Dorogoy, A. Geometrical Imperfection and Adiabatic Shear Banding. *Int. J. Impact Eng.* **2008**, *35*, 1280–1292. [CrossRef]
12. Goviazin, G.G.; Rittel, D. Revisiting the Hot Adiabatic Shear Band Paradigm. *Int. J. Impact Eng.* **2023**, *180*, 104702. [CrossRef]
13. Rittel, D.; Wang, Z.G.; Merzer, M. Adiabatic Shear Failure and Dynamic Stored Energy of Cold Work. *Phys. Rev. Lett.* **2006**, *96*, 075502. [CrossRef]
14. Uçak, N.; Aslantas, K.; Çiçek, A. The Effects of Al2O3 Coating on Serrated Chip Geometry and Adiabatic Shear Banding in Orthogonal Cutting of AISI 316L Stainless Steel. *J. Mater. Res. Technol.* **2020**, *9*, 10758–10767. [CrossRef]
15. Gu, L. Mechanism Study on Adiabatic Shear Fracture Induced Isolated Segment Formation during High-Speed Machining. *Procedia CIRP* **2018**, *77*, 348–350. [CrossRef]
16. Guohe, L.; Minjie, W.; Chunzheng, D. Adiabatic Shear Critical Condition in the High-Speed Cutting. *J. Mater. Process. Technol.* **2009**, *209*, 1362–1367. [CrossRef]
17. Winter, S.; Nestler, M.; Galiev, E.; Hartmann, F.; Psyk, V.; Kräusel, V.; Dix, M. Adiabatic Blanking: Influence of Clearance, Impact Energy, and Velocity on the Blanked Surface. *J. Manuf. Mater. Process.* **2021**, *5*, 35. [CrossRef]
18. Linnemann, M.; Scheffler, C.; Psyk, V. Numerically Assisted Design For Electromagnetically Driven Tools. *Procedia Manuf.* **2020**, *47*, 1334–1338. [CrossRef]
19. Yaldız, S.; Sağlam, H.; Ünsaçar, F.; Işık, H. Design and Applications of a Pneumatic Accelerator for High Speed Punching. *Mater. Des.* **2007**, *28*, 889–896. [CrossRef]
20. Mottram, A.R. High Energy Rate Forming Techniques. In *Mechanical Engineer's Reference Book*; Elsevier: Amsterdam, The Netherlands, 1973; pp. 9-2–9-16.
21. Vivek, A.; Daehn, G.S. Vaporizing Foil Actuator: A Versatile Tool for High Energy-Rate Metal Working. *Procedia Eng.* **2014**, mboxemph81, 2129–2134. [CrossRef]
22. Rehm, M.; Ihlenfeldt, S.; Schlegel, H.; Drossel, W.-G. Mechanically Coupled High Dynamic Linear Motors—A New Design Approach and Its Control Strategy. *CIRP Ann.* **2014**, *63*, 381–384. [CrossRef]
23. Kalpakjian, S.; Schmid, S.R. *Manufacturing Processes for Engineering Materials*, 6th ed.; Pearson: London, UK, 2016; ISBN 978-0134290553.
24. Bernstein, H. Gleichstrom-, Schritt- Und Linearmotoren. In *Elektrotechnik/Elektronik für Maschinenbauer*; Springer Fachmedien Wiesbaden GmbH: Wiesbaden, Germany, 2018; pp. 289–329.
25. Eller, C. Kinetik Des Massenpunktsystems. In *Holzmann/Meyer/Schumpich Technische Mechanik Kinematik und Kinetik*; Springer Fachmedien Wiesbaden GmbH: Wiesbaden, Germany, 2019; pp. 155–168.
26. VDI 2906 Blatt 2 Schnittflächenqualität beim Schneiden, Beschneiden und Lochen von Werkstücken aus Metall; Scherschneiden. VDI-Handbuch Produktionstechnik und Fertigungsverfahren—Band 2: Fertigungsverfahren, 1994.
27. Galiev, E.; Winter, S.; Reuther, F.; Psyk, V.; Tulke, M.; Brosius, A.; Kräusel, V. Local Temperature Development in the Fracture Zone during Uniaxial Tensile Testing at High Strain Rate: Experimental and Numerical Investigations. *Appl. Sci.* **2022**, *12*, 2299. [CrossRef]
28. Feucht, M.; Neukamm, F.; Haufe, A. A Phenomenological Damage Model to Predict Material Failure in Crashworthiness Applications. In *Recent Developments and Innovative Applications in Computational Mechanics*; Springer: Berlin/Heidelberg, Germany, 2011; pp. 143–153.
29. Psyk, V.; Scheffler, C.; Tulke, M.; Winter, S.; Guilleaume, C.; Brosius, A. Determination of Material and Failure Characteristics for High-Speed Forming via High-Speed Testing and Inverse Numerical Simulation. *J. Manuf. Mater. Process.* **2020**, *4*, 31. [CrossRef]